Emission Spectroscopic Characterization of a Helium Atmospheric Pressure Plasma Jet with Various Mixtures of Argon Gas in the Presence and the Absence of De-Ionized Water as a Target

Nima Bolouki [1],* , Jang-Hsing Hsieh [1,2], Chuan Li [3] and Yi-Zheng Yang [2]

[1] Center for Plasma and Thin Film Technologies, Ming Chi University of Technology,
    New Taipei City 24301, Taiwan
[2] Department of Materials Engineering, Ming Chi University of Technology, New Taipei City 24301, Taiwan
[3] Department of Biomedical Engineering, National Yang Ming University, Taipei 112-21, Taiwan
* Correspondence: bolouki@mail.mcut.edu.tw

Abstract: A helium-based atmospheric pressure plasma jet (APPJ) with various flow rates of argon gas as a variable working gas was characterized by utilizing optical emission spectroscopy (OES) alongside the plasma jet. The spectroscopic characterization was performed through plasma exposure in direct and indirect interaction with and without de-ionized (DI) water. The electron density and electron temperature, which were estimated by Stark broadening of atomic hydrogen (486.1 nm) and the Boltzmann plot, were investigated as a function of the flow rate of argon gas. The spectra obtained by OES indicate that the hydroxyl concentrations reached a maximum value in the case of direct interaction with DI water as well as upstream of the plasma jet for all cases. The relative intensities of hydroxyl were optimized by changing the flow rate of argon gas.

Keywords: atmospheric pressure plasma jet; plasma characterization; optical emission spectroscopy

1. Introduction

Cold atmospheric plasma devices, mainly based on the atmospheric pressure plasma jet (APPJ) [1], have emerged over recent decades. Such devices offer the possibility of direct and indirect (remote) methods for bacteria inactivation [2], biofilm control [3], cancer cell treatment [4], water purification [5], plasma activated water [6], and so on. The APPJ with a tube-shaped configuration fed by helium gas was presented by Laroussi et al. [7] for the first time. Then, the APPJ was developed and extended with different electrode configurations and working gases.

Generally, an APPJ with various mixtures of feed gases provides numerous types of reactive species with different concentrations [8,9]. One of the species is a hydroxyl radical, which provides excellent benefits for biological and medical applications although it has a short lifetime [10,11]. Some articles reported the characterization of the argon-based APPJ with a mixture of water to enhance the hydroxyl species [12–14]. Argon as a working gas might be considered as an alternative candidate since scarce and costly helium is consumed in a large volume in the APPJ. The argon APPJ has better energy transfer efficiency compared to the helium jet; however, it releases considerable heat [15]. The conditions of electrical discharges in a pure argon gas might be unstable as a result of changing the parameters related to experimental conditions. For example, an additive gas such as oxygen is able to extinguish the argon discharge and shrink the range of discharge stabilities due to low electron temperature compared to the helium discharge [15,16]. Therefore, a plan of mixing argon and helium

gases is proposed not only to reduce helium consumption but also to enhance the concentration of reactive species, specifically hydroxyl.

Based on the specific applications, the APPJ-based devices are designed and constructed with different power sources, geometries, and working gases, which results in changing the electrical conditions of the APPJ as well as the produced reactive species. Moreover, interactions of the plasma jet with liquid targets, which are most of the biological cases, influence the plasma conditions and the produced reactive species. Therefore, it is undoubtedly necessary to measure the plasma parameters to characterize a homemade APPJ in interaction with liquid.

Optical emission spectroscopy (OES) [17], as an affordable and a non-intrusive diagnostics method with an easy experimental setup, is used to identify the plasma parameters and reactive species produced by an APPJ. In this case, the radiations emitted by excited atoms, molecules, and reactive species in the plasma source are collected and analyzed to determine the plasma parameters, such as electron density, electron temperature, gas temperature, and so on. The Boltzmann plot [18] is an established method to estimate the electron temperature by assuming that the plasma condition is in a state of partial local thermodynamic equilibrium due to high collision frequency between particles in atmospheric pressure [19]. The upper levels of the atomic transitions follow the Saha–Boltzmann distribution. Hence, the excitation and electron temperatures are assumed to be the same, although this is an inappropriate assumption in mid and low pressures [20,21]. Stark broadening of the Balmer series lines of atomic hydrogen (H_α, H_β, H_γ) [18], which are broadenings or shifts of the spectral lines due to the presence of the electric fields of charged particles, allows us to calculate the electron density in atmospheric pressure. Electron density is almost independent of electron temperature for a given broadening of the H_β line, while in the cases of H_α and H_γ, this dependency is obvious specifically for H_α [22]. Therefore, the H_β broadening (486.1 nm) is utilized to diagnose the electron density. The Stark broadening can be considered as a reliable method for the values of electron density higher than 10^{19} m^{-3}. Otherwise, less than this value, the contributions of Doppler and Van der Waals would be dominant, leading to a high error range in the estimation of electron density [23].

In addition to measurements of electron density and electron temperature, the neutral gas temperature plays a vital role in plasma characterization and processes. For instance, in biological applications, the high gas temperature of the APPJ is capable of damaging biological cells and tissues. Generally, there is no specific threshold temperature for heating damage, which depends on the type of biological cells and tissues; however, in biological testing, the temperature should be less than 42 °C [24]. Therefore, to confirm whether the APPJ might be suitable for the desired application, measurements of the gas temperature would be necessary. Also, to estimate the electron density by the Stark effect, the contributions of Van der Waals and Doppler broadenings, which depend on the gas temperature, should be considered. Hence, knowing the gas temperature is needed. In atmospheric pressure, it is assumed that the rotational temperature of the second positive system of nitrogen gas is equal to the neutral gas temperature [25].

In this study, to characterize and optimize the APPJ, the relative intensities of reactive excited species have been measured using OES. The electron temperature has been estimated by the Boltzmann plot alongside the plasma jet. Since the Balmer series line of atomic hydrogen has been too weak, the measurements of Stark broadening have been carried out at the bottom of the plasma jet. While the flow rate of helium gas is held constant, the influences of argon gas with various flow rates on relative intensities of species and plasma parameters in the presence and the absence of de-ionized (DI) water as a target have been investigated upstream, midstream, and downstream of the plasma jet. The rotational temperature of the second positive system of nitrogen gas has been measured to estimate the neutral gas temperature downstream of the plasma jet in direct interaction with DI water.

2. Materials and Methods

2.1. Experimental Setup of the Atmospheric Pressure Plasma Jet

The experimental setup of the APPJ is shown in Figure 1. The setup consists of a quartz tube with two copper electrodes in a cylindrical shape with a gap distance of 15 mm. A high voltage DC pulsed power supply delivers a monopolar pulsed voltage with a square wave-form pulse. The on-time and off-time of the pulsed voltage were adjusted to be 25 μs, while the rise and fall time was adjusted to be 3 μs. A voltage probe (Rigol-RP1018H) and a current probe (Cybertek-CP8030B) were used to measure the applied voltage and the plasma current. The voltage and current waveform were recorded using an oscilloscope (Rigol DS1054z, 50 MHz, 1 GS/s). During the experiment, helium as a working gas with the flow rate of 5 slm (standard liter/min) remained unchanged, while the argon flow rate as a variable parameter of the working gas was controlled and adjusted to be 0–2000 sccm (standard cubic centimeter/min) by mass flow controller (MFC). The experiments based on the target situation were carried out in three cases. The first case represents the APPJ without de-ionized (DI) water. The second and third cases refer to the presence of DI water as a target exposed by the APPJ directly and indirectly. The maximum distance between the downstream position of the APPJ and the surface of DI water in the case of the indirect plasma exposure was selected to be 4 mm. The APPJ was mounted on an adjustable stage and, thus, the distance of 4 mm was adjusted by the stage.
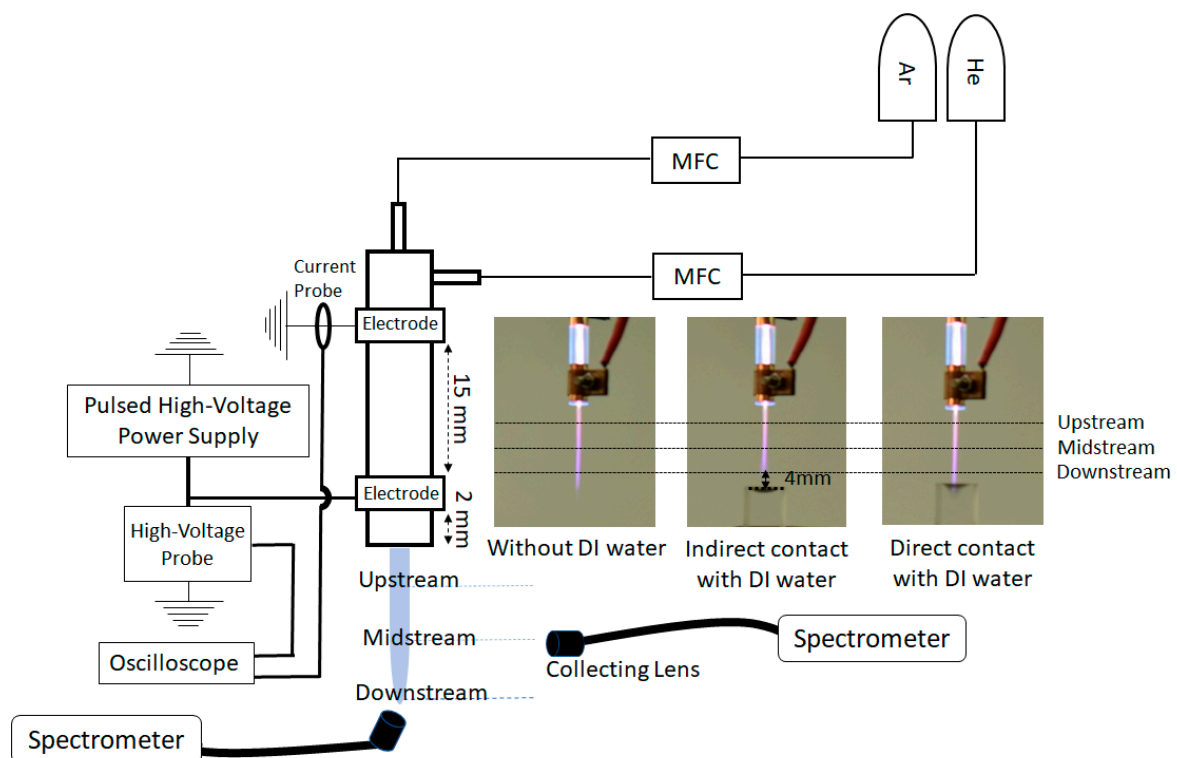
Figure 1. Experimental setup of the helium APPJ with various flow rates of argon gas. The spectroscopic characterization was performed alongside the plasma jet in direct and indirect interaction with and without DI water.

2.2. Electrical Measurements

Figure 2 shows the voltage and current characteristics of the discharge. The maximum values of applied pulsed voltage and frequency were adjusted to be 8.5 kV and 17.8 kHz, respectively. The flow rate of argon gas of the recorded voltage and current was 1600 sccm. It should be noted that the voltage–current waveform was examined with different flow rates of argon gas. The waveform of the discharge did not change significantly.
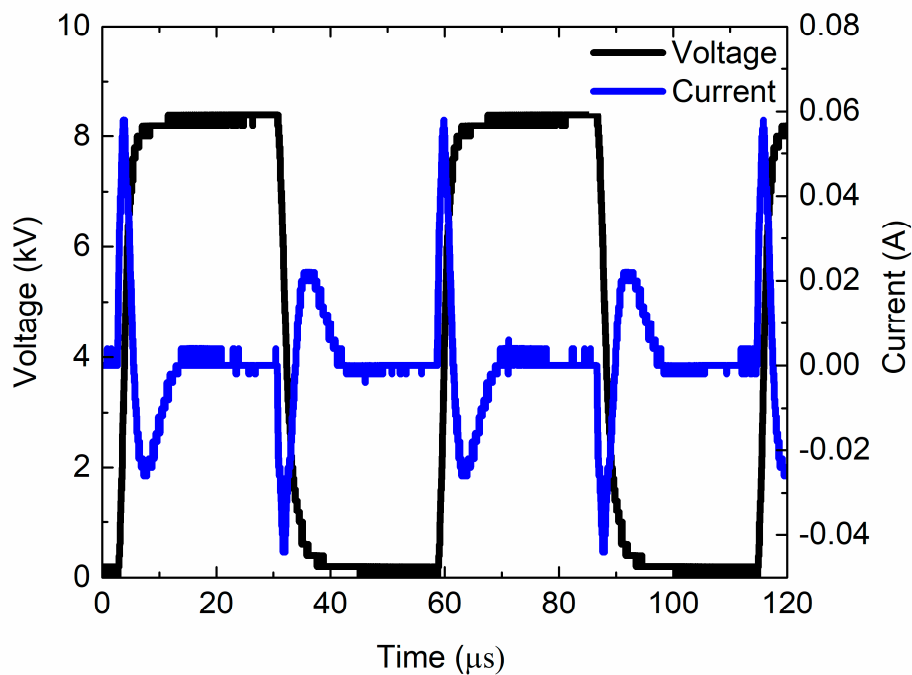
Figure 2. Voltage–current characteristic of the helium-based APPJ with the flow rate of 1600 sccm of argon gas.

2.3. Spectroscopic Measurements

The emission spectra of the APPJ was measured using a spectrometer (Avantes, AvaSpec-2048L, focal length of 75 mm, grating with line density of 300 mm^{-1}, entrance slit of 25 μm, 2048-pixel CCD detector) with a spectral range of 200–1100 nm and a spectral resolution of 1.4 nm. A fiber optics cable including a collecting lens was used to capture the light emitted from the APPJ. The emission spectra were recorded for 5 accumulations with an exposure time of 100 ms. The measuring points of the electron temperature were selected to be upstream, midstream, and downstream of the APPJ as shown in Figure 1. Since the hydrogen Balmer line in the wavelength of 486.1 nm (H$_\beta$) was too weak to be detected in the plasma jet, the spectrometer was placed at the bottom of the plasma jet to enhance the signal intensity of Stark broadening related to the hydrogen Balmer line for measuring the electron density.

3. Results and Discussion

3.1. Measurements of Relative Intensities of Species

Figure 3 presents the spectra of optical emission of the plasma jet obtained by OES in the cases of non-contact (free of DI water—Figure 3a,b), indirect contact (Figure 3c,d), and direct contact (Figure 3e,f) with DI water. The spectra were measured with and without argon feed gas (flow rate of 1600 sccm) downstream and upstream of the jet stream. Hydroxyl (309 nm), helium (706 nm), and argon (750 nm) species, as well as the second positive system of nitrogen gas, were identified in the spectra. As mentioned before and shown in the figure, in all cases, the hydrogen Balmer line (H$_\beta$) is too weak to estimate the electron density.
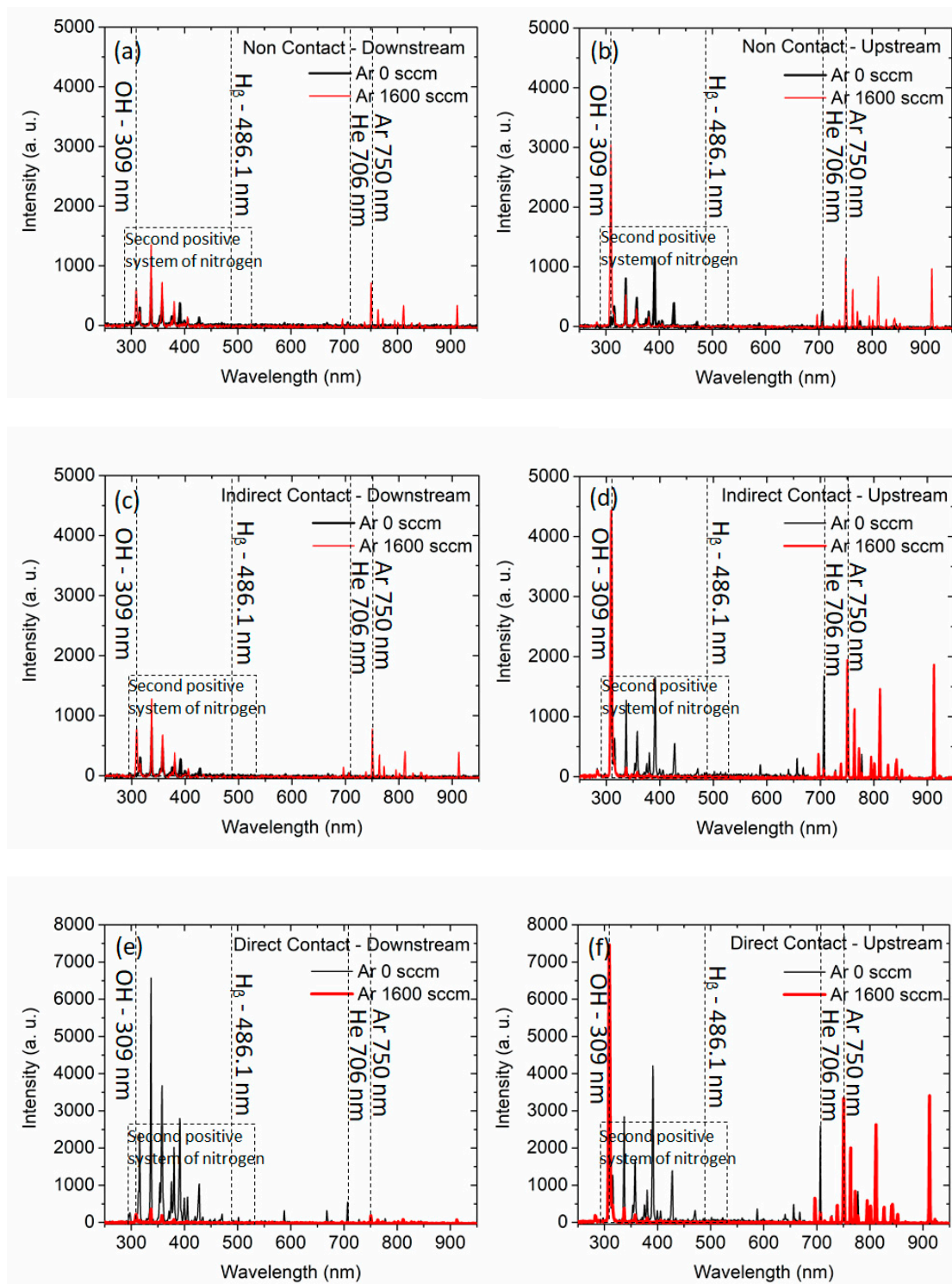
Figure 3. The emission spectra of the plasma jet with and without argon gas in the cases of (**a**) and (**b**) non-contact, (**c**) and (**d**) indirect contact with DI water, and (**e**) and (**f**) direct contact with DI water. The measurements have been performed at the downstream and the upstream of the plasma jet.

Figure 4 shows the spatial profile of relative intensities of hydroxyl (309 nm), helium (706 nm), and argon (750 nm) species of the APPJ obtained by OES with different flow rates of argon gas in the cases of free of DI water (Figure 4a), and indirect contact (Figure 4b) and direct contact with DI water (Figure 4c). The figure shows that relative intensities of hydroxyl are higher upstream of the jet compared to the other measured positions for all cases. In the case of the indirect contact with DI

water, shown in Figure 4b, the relative intensity of hydroxyl increases more. The enhancement of the hydroxyl concentration is boosted in the case of direct contact with DI water alongside the plasma jet. The intensity value of hydroxyl species rises more than two times compared to the case of free of DI water by considering the values shown in Figure 4a,c. Moreover, the relative intensities of hydroxyl species reach the maximum amount at the flow rate of 1600 sccm specifically at the upstream of the plasma jet; then, the intensities of hydroxyl decrease for all cases. In the case of direct contact, at the flow rate of 2000 sccm, the spectrum was not available to measure the intensities of the species as the length of the plasma jet decreased to half. Since the flow rate of helium gas was held constant during the experiment, the intensities of helium species remained nearly unchanged, as shown in Figure 4, for all cases.
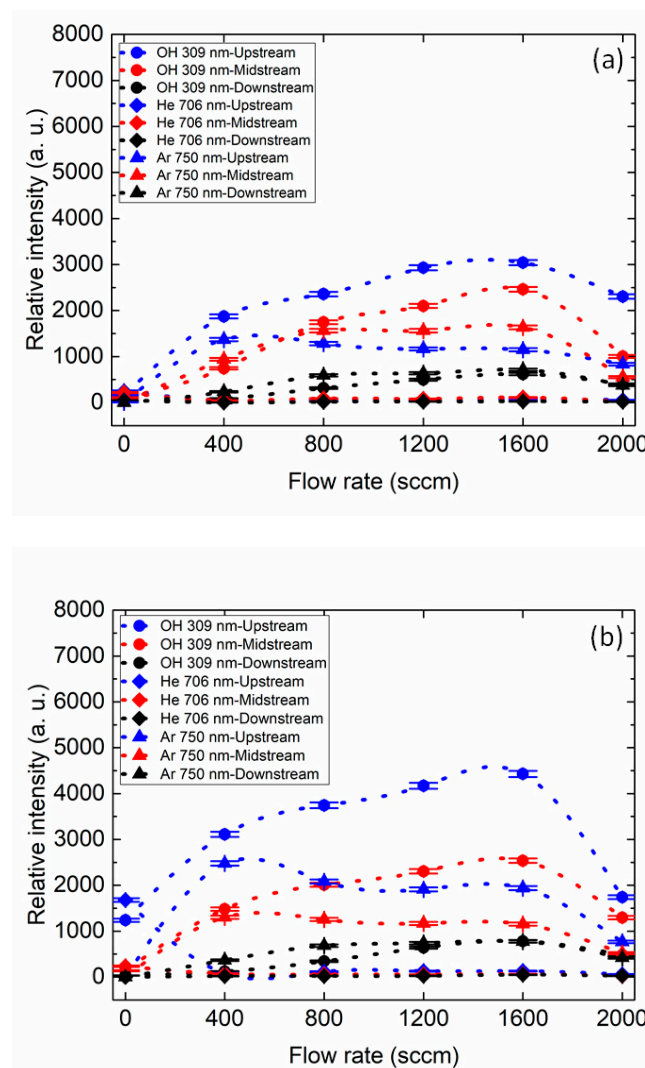
Figure 4. *Cont.*
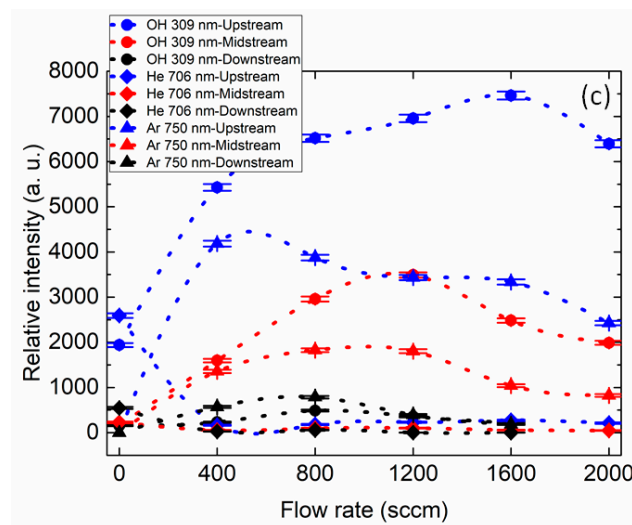
Figure 4. The relative intensity of hydroxyl (309 nm), helium (706 nm), and argon (750 nm) obtained by OES as a function of the flow rate of argon gas in the cases of (**a**) non-contact with DI water; (**b**) indirect contact with DI water; and (**c**) direct contact of DI water.

3.2. Measurements of Gas Temperature

Although the second positive system of nitrogen bands were obvious in all cases (Figure 3), the intensity of the second positive system was strong without argon gas feed in the case of direct contact with DI water as shown in Figure 3e,f. As mentioned above, the nitrogen band allows us to measure the temperature of the neutral particle based on the rotational temperature of nitrogen gas. By fitting the emission line spectra of the second positive system (C $^3\Pi_u$ → B $^3\Pi_g$ = 375–381 nm) [26], the gas temperature was measured to be 0.03 eV, equal to 75 °C. Thus, the APPJ is in the non-thermal state and regarded as a cold plasma. In addition, the ambient temperature was measured by a mercury thermometer at a distance of around 10 mm from the tip of the plasma jet for 2 minutes. The temperature was recorded to be 33.2 °C.

3.3. Measurements of Electron Density and Electron Temperature

Figure 5 illustrates the spatial profile of the electron temperature estimated by the Boltzmann plot upstream, midstream, and downstream of the APPJ in the cases of free of DI water (Figure 5a), and indirect (Figure 5b) and direct contact with DI water (Figure 5c). The measured parameters are plotted with different flow rates of argon gas. The estimated electron density based on Stark broadening in the case of free of DI water (no target) is shown in Figure 5a. At the flow rate of 400 sccm, the electron density and the electron temperature were estimated to be 1.2×10^{22} m^{-3} and 0.25–0.45 eV alongside the plasma jet. The electron density reached the maximum value of 2.3×10^{22} m^{-3} at the flow rate of 1600 sccm, then decreased to the flow rate of 2000 sccm. However, the trend of electron temperature was downward between the flow rates of 400 to 2000 sccm, and finally, reached the values of 0.15–0.21 eV at the flow rate of 2000 sccm. Injecting the massive species to the plasma discharge leads to a change in the energy transfer between electrons and the species due to the collision frequency that causes a reduction in electron temperature. The electron temperature converges more by increasing the flow rate of argon gas in the case of direct contact; nevertheless, the trend of electron temperature is almost the same for all cases. In the case of direct contact, at the flow rate of 2000 sccm, the spectrum was not available to estimate the electron temperature as the length of the plasma jet decreased to half.
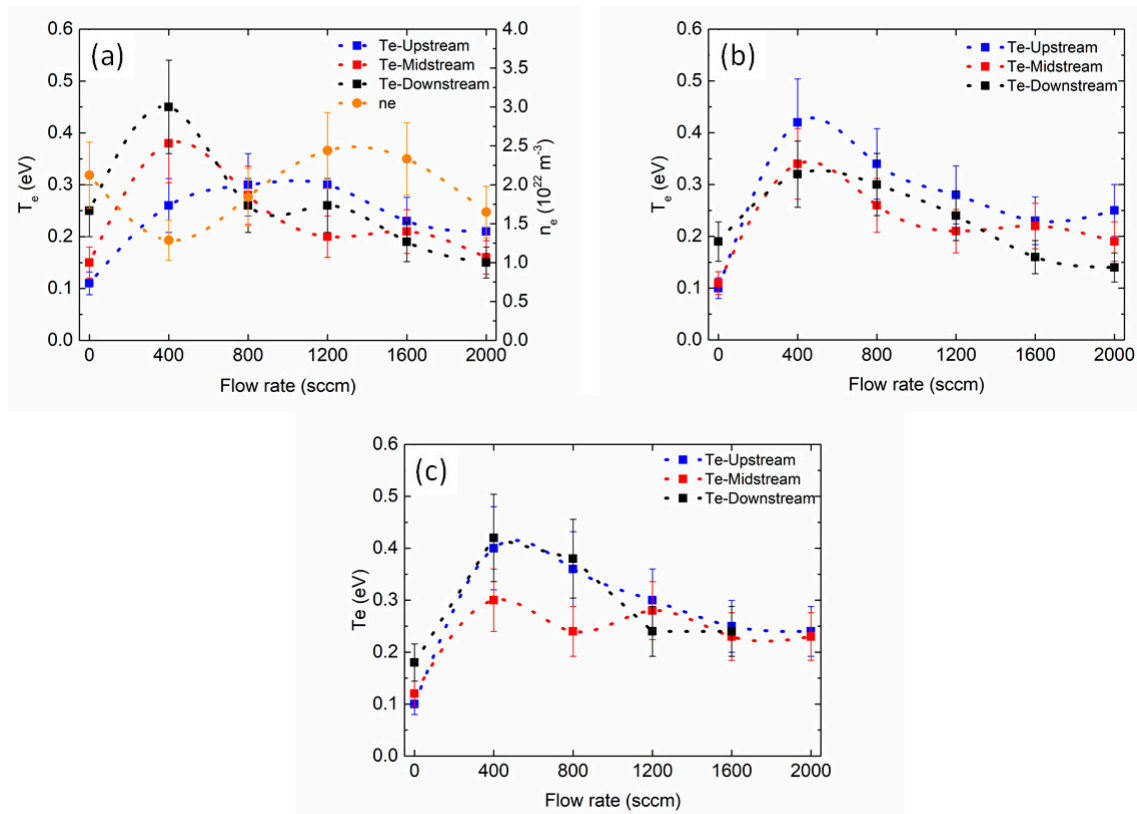
Figure 5. Spatial profile measurements of the electron temperature upstream, midstream, and downstream of the APPJ in the cases of (**a**) non-contact with DI water; (**b**) indirect contact with DI water; and (**c**) direct contact of DI water. Measurement of electron density was undertaken at the bottom of the jet stream.

The Boltzmann plot equation is assumed to be $\ln(I\lambda/gA) = -E/kT_e + \text{constant}$, where I is the measured intensity obtained by OES, λ is the selected wavelength associated with helium and argon gases, g is the statistical weight, A is the transition probability, E is the excitation energy corresponding to the selected wavelengths, k is Boltzmann constant, and T_e is electron temperature. The selected wavelengths of atomic emission lines related to argon and helium gases were obtained from references [12,27] to estimate the electron temperature based on the Boltzmann plot. The spectroscopic data related to the wavelengths of excited atoms and ions were confirmed via the NIST atomic database [28]. By adding argon gas, the contributed wavelengths of helium [27] for the estimation of electron temperature weakened; therefore, the wavelengths of argon [12] were used at the flow rate of 400 to 2000 sccm.

Regarding Stark broadening, although hydrogen gas was not used as a working gas in the APPJ, it initially might result from the impurity of helium and argon working gases or the ambient air. The relationship between electron density and Stark broadening is assumed to be $n_e = (\Delta\lambda_{FWHM}/(2 \times 10^{-11}))^{3/2}$, where $\Delta\lambda_{FWHM}$ is Stark broadening and n_e is electron density in terms of per cubic centimeter. The broadening of the spectral line is a convolution of instrumental, Doppler, and Van der Waals broadenings [29]. The Voigt fitting of the measured Stark bordering was performed using Origin Pro 5. The instrumental broadening was obtained by replacing the APPJ with a mercury lamp (wavelength of 546.1 nm) at low pressure. This value was obtained to be 0.06 nm. Finally, the Voigt fitting was excluded from the broadenings mentioned above to estimate the pure Stark broadening at full width at half maximum (FWHM) for measurements of electron density.

The presence of massive particles such as argon species in the helium plasma changes the plasma chemistry and the degree of ionization. Based on the results of relative intensities of excited species obtained by OES, the hydroxyl concentration is highest upstream of the plasma jet compared to the

other regions. The production of hydroxyl might be explained by two possible different mechanisms of reactions [30]. The first mechanism corresponds to the direct dissociation of the water molecule by energetic electrons. Based on the results, by increasing the flow rate, the electron temperature drops. So, the energy of the electrons is too low (less than 1 eV) to dissociate the water molecule. The second refers to the possibility of participation of metastable argon to produce H_2O^+. In this case, the dissociative recombination of H_2O^+ leads to hydroxyl generation. Therefore, the metastable atoms may play an important role to generate hydroxyls [14,31]. That is the reason the concentration of hydroxyl is highest upstream of the plasma jet for all cases, as the concentration of the metastable species of argon is highest in the same space. In addition, as the plasma jet approaches the water surface, the humidity around the plasma jet enhances due to the water evaporation that causes a boost of hydroxyl generation in the presence of water. Yang et al. [30] reported similar results by using the helium-based APPJ with the fixed flow rate of helium gas, while in our case, the flow rate of the APPJ changed by argon gas.

4. Conclusions

We characterized and optimized a helium APPJ with a mixture of argon gas in the presence and the absence of DI water. DI water as a target was exposed by the APPJ directly and indirectly. Electron temperature and electron density as a function of the flow rate of the gas mixtures were investigated. In a direct interaction of the jet stream and surface of DI water, the gas temperature was estimated based on the rotational temperature to confirm the plasma condition is in the non-thermal regime. The OES results show that approaching the APPJ so that the jet stream would have an indirect interaction with the water surface leads to more hydroxyl concentration with respect to the free plasma case. Hydroxyl production could be boosted more in direct contact with DI water. Considering positive points and drawbacks of using pure helium or argon gases to produce the APPJ, mixing these two gases might be the right solution for biological and environmental applications.

Conflicts of Interest: The authors declare no conflict of interest.

References

1. Winter, J.; Brandenburg, R.; Weltmann, K.-D. Atmospheric pressure plasma jets: An overview of devices and new directions. *Plasma Source Sci. Technol.* **2015**, *24*, 064001. [CrossRef]
2. Pedroni, M.; Morandi, S.; Silvetti, T.; Cremona, A.; Gittini, G.; Nardone, A.; Pallotta, F.; Brasca, M.; Vassallo, E. Bacteria inactivation by atmospheric pressure plasma jet treatment. *J. Vac. Sci. Technol.* **2017**, *36*, 01A107. [CrossRef]
3. Gilmore, B.F.; Flynn, P.B.; Brien, S.O.; Hickok, N.; Freeman, T.; Bourke, P. Cold plasmas for biofilm control: Opportunities and challenges. *Trends Biotechnol.* **2018**, *36*, 627–628. [CrossRef] [PubMed]
4. Keidar, M.; Shashurin, A.; Volotskova, O.; Stepp, M.A.; Srinivasan, P.; Sandler, A.; Trink, B. Cold atmospheric plasma in cancer therapy. *Phys. Plasmas* **2013**, *20*, 057101. [CrossRef]
5. Foster, J.E. Plasma-based water purification: Challenges and prospects for the future. *Phys. Plasmas* **2017**, *24*, 055501. [CrossRef]
6. Thirumdas, R.; Kothakota, A.; Annapure, U.; Siliveru, K.; Blundell, R.; Gatt, R.; Valdramidis, V.P. Plasma activated water (PAW): Chemistry, physio-chemical properties, applications in food and agriculture. *Trends Food Sci. Technol.* **2018**, *77*, 21–31. [CrossRef]
7. Laroussi, M.; Lu, X. Room-temperature atmospheric pressure plasma plume for biomedical applications. *Appl. Phys. Lett.* **2005**, *87*, 113902. [CrossRef]
8. Bruggeman, P.; Brandenburg, R. Atmospheric pressure discharge filaments and microplasmas: Physics, chemistry and diagnostics. *J. Phys. D Appl. Phys.* **2013**, *46*, 464001. [CrossRef]

9.   Santosh, V.S.; Kondetia, K.; Phanb, C.Q.; Wendec, K.; Jablonowskic, H.; Gangala, U.; Granickd, J.L.; Hunterb, R.C.; Bruggemana, P.J. Long-lived and short-lived reactive species produced by a cold atmospheric pressure plasma jet for the inactivation of Pseudomonas aeruginosa and Staphylococcus aureus. *Free Radic. Biol. Med.* **2018**, *124*, 275–287. [CrossRef]

10.   Liu, C.T.; Wu, C.J.; Yang, Y.W.; Lin, Z.H.; Wu, J.S.; Hsiao, S.C.; Lin, C.P. Atomic Oxygen and Hydroxyl Radical Generation in Round Helium-Based Atmospheric-Pressure Plasma Jets by Various Electrode Arrangements and Its Application in Sterilizing Streptococcus mutans. *IEEE Trans. Plasma Sci.* **2014**, *42*, 12. [CrossRef]

11.   Yue, Y.F.; Mohades, S.; Laroussi, M.; Lu, X. Measurements of Plasma-Generated Hydroxyl and Hydrogen Peroxide Concentrations for Plasma Medicine Applications. *IEEE Trans. Plasma Sci.* **2016**, *44*, 11. [CrossRef]

12.   Sarani, A.; Nikiforov, A.Y.; Leys, C. Atmospheric pressure plasma jet in Ar and Ar/H2O mixtures: Optical emission spectroscopy and temperature measurements. *Phys. Plasmas* **2010**, *17*, 063504. [CrossRef]

13.   Cheng, C.; Shen, J.; Xiao, D.-Z.; Xie, H.-B.; Lan, Y.; Fang, S.-D.; Meng, Y.-D.; Chu, P.K. Atmospheric pressure plasma jet utilizing Ar and Ar/H2O mixtures and its applications to bacteria inactivation. *Chin. Phys. B* **2014**, *23*, 0752204. [CrossRef]

14.   Nikiforov, A.Y.; Sarani, A.; Leys, C. The influence of water vapor content on electrical and spectral properties of an atmospheric pressure plasma jet. *Plasma Source Sci. Technol.* **2011**, *20*, 015014. [CrossRef]

15.   Wang, S.; Schulz-von der Gathen, V.; Döbele, H.F. Discharge comparison of nonequilibrium atmospheric pressure Ar/O2 and He/O2 plasma jets. *Appl. Phys. Lett.* **2003**, *83*, 16. [CrossRef]

16.   Li, S.-Z.; Lim, J.-P.; Kang, J.G.; Uhm, H.S. Comparison of atmospheric-pressure helium and argon plasmas generated by capacitively coupled radio-frequency discharge. *Phys. Plasmas* **2006**, *13*, 093503. [CrossRef]

17.   Fantz, U. Basic of plasma spectroscopy. *Plasma Source Sci. Technol.* **2006**, *15*, S137–S147. [CrossRef]

18.   Griem, H.R. *Plasma Spectroscopy*; McGraw-Hill: New York, NY, USA, 1964.

19.   Calzada, M.D.; Moisan, M.; Gamero, A.; Sola, A. Experimental investigation and characterization of the departure from local thermodynamic equilibrium along a surface-wave-sustained discharge at atmospheric pressure. *J. Appl. Phys.* **1996**, *80*, 46. [CrossRef]

20.   Sola, A.; Calzada, M.D.; Gamero, A. On the use of the line-to-continuum intensity ratio for determining the electron temperature in a high-pressure argon surface-microwave discharge. *J. Phys. D Appl. Phys.* **1995**, *28*, 4. [CrossRef]

21.   Gordillo-Vázquez, F.J.; Camero, M.; Gómez-Aleixandre, C. Spectroscopic measurements of the electron temperature in low pressure radiofrequency Ar/H2/C2H2 and Ar/H2/CH4 plasmas used for the synthesis of nanocarbon structures. *Plasma Sources Sci. Technol.* **2005**, *15*, 1. [CrossRef]

22.   Torres, J.; Palomares, J.M.; Sola, A.; van der Mullen, J.J.A.M.; Gamero, A. A Stark broadening method to determine simultaneously the electron temperature and density in high-pressure microwave plasmas. *J. Phys. D Appl. Phys.* **2007**, *40*, 5929–5936. [CrossRef]

23.   Zhu, X.M.; Pu, Y.K.; Balcon, N.; Boswell, R. Measurement of the electron density in atmospheric-pressure low-temperature argon discharges by line-ratio method of optical emission spectroscopy. *J. Phys. D Appl. Phys.* **2009**, *42*, 142003. [CrossRef]

24.   Yarmolenko, P.S.; Moon, E.J.; Landon, C.; Manzoor, A.; Hochman, D.W.; Viglianti, B.L.; Dewhirst, M.W. Thresholds for thermal damage to normal tissues: An update. *Int. J. Hyperth.* **2011**, *27*, 320–343. [CrossRef] [PubMed]

25.   Masoud, N.; Martus, K.; Figus, M.; Becker, K. Rotational and Vibrational Temperature Measurements in a High-Pressure Cylindrical Dielectric Barrier Discharge (C-DBD). *Contrib. Plasma Phys.* **2005**, *45*, 30–37. [CrossRef]

26.   Koike, S.; Sakamoto, T.; Kobori, H.; Matsuura, H.; Akatsuka, H. Spectroscopic Study on Vibrational Nonequilibrium of a Microwave Discharge Nitrogen Plasma. *Jpn. J. Appl. Phys.* **2004**, *43*, 5550. [CrossRef]

27.   Gulec, A.; Bozduman, F.; Hala, A.M. Atmospheric pressure 2.45-GHz microwave helium plasma. *IEEE Trans. Plasma Sci.* **2015**, *43*, 786790. [CrossRef]

28.   NIST Atomic Spectra Database. Available online: http://physics.nist.gov/PhysRefData (accessed on 21 February 2019).

29.   Ouyang, Z.; Surla, V.; Cho, S.T.; Ruzic, D.N. Characterization of an atmospheric-pressure helium plasma generated by 2.45-GHz microwave power. *IEEE Trans. Plasma Sci.* **2012**, *40*, 3476–3481. [CrossRef]

30. Yang, Y.; Zhang, Y.; Liao, Z.; Pei, X.; Wu, S. OH Radicals Distribution and Discharge Dynamics of an Atmospheric Pressure Plasma Jet above Water Surface. *IEEE Trans. Radiat. Plasma Med. Sci.* **2018**, *2*, 223–228. [CrossRef]

31. Collette, A.; Dufour, T.; Reniers, F. Reactivity of water vapor in an atmospheric argon flowing post discharge plasma torch. *Plasma Sources Sci. Technol.* **2016**, *25*, 025014. [CrossRef]